Geomechanics for Energy and the Environment 2 (2015) 32–44

Contents lists available at ScienceDirect

Geomechanics for Energy and the Environment

journal homepage: www.elsevier.com/locate/gete

Integrated hydro-mechanical and seismic modelling of the Valhall reservoir: A case study of predicting subsidence, AVOA and microseismicity

D.A. Angus [a,*], M. Dutko [b], T.G. Kristiansen [c], Q.J. Fisher [a], J.-M. Kendall [d], A.F. Baird [d], J.P. Verdon [d], O.I. Barkved [c,1], J. Yu [b], S. Zhao [b]

[a] University of Leeds, Leeds, UK
[b] Rockfield Software Ltd, Swansea, UK
[c] BP, Stavanger, Norway
[d] University of Bristol, Bristol, UK

HIGHLIGHTS

- We integrate fluid-flow, geomechanical and seismic modelling to the Valhall reservoir.
- We predict surface subsidence, seismic anisotropy and microseismicity and compare with field observations.
- The results are consistent with observation and indicate that the integrated approach can add value to model calibration.

ARTICLE INFO

Article history:
Received 14 November 2014
Received in revised form 19 May 2015
Accepted 19 May 2015
Available online 28 May 2015

Keywords:
AVOA
Coupled fluid-flow and geomechanics
Microseismicity
Rock physics
Subsidence

ABSTRACT

Geomechanical, fluid-flow and seismic modelling have been combined to predict surface subsidence, seismic anisotropy and microseismicity for the Valhall reservoir, North Sea. The constitutive model used in the geomechanical simulation consists primarily of layers having poro-elastic behaviour, but with poro-elasto-plasticity behaviour in the chalk reservoir units. The constitutive model incorporates matrix deformation during simulation, such that areas of compaction and dilation are modelled so that the likely microseismic response of the reservoir can be predicted. In the coupled fluid-flow and geomechanical (hydro-mechanical) workflow, a finite-element geomechanical simulator is coupled to a reservoir fluid-flow simulator and applied to predict seafloor subsidence. Subsequently, the history-matched hydro-mechanical results are transformed into dynamic elastic models suitable for seismic analysis using an empirical static-to-dynamic relationship and stress-dependent rock physics model. The elastic models are then used to predict seismic anisotropy and microseismicity, allowing for an additional assessment of hydro-mechanical simulation via comparison with observed field seismic data. The geomechanical model has been calibrated to reproduce the measured subsidence. Furthermore, the predicted seismic anisotropy extracted from the reflection amplitude variation with offset and azimuth resembles that measured from field seismic data, despite the limited calibration of the rock physics model to the Valhall reservoir rocks. The spatial pattern of modelled microseismicity is consistent with previously published microseismic analyses, where the modelled failure mechanisms are consistent with typical production-induced seismicity.

* Corresponding author.
E-mail address: d.angus@leeds.ac.uk (D.A. Angus).
[1] Current address: Petoro AS, Øvre Strandgate 124, 4002 Stavanger, Norway.

http://dx.doi.org/10.1016/j.gete.2015.05.002

The results of this study indicate that seismic data has the potential to improve the calibration of hydro-mechanical models beyond what is possible from conventional fluid production and surface subsidence data. This is significant as seismic data could provide greater control over the whole field rather than borehole and surface measurements.

1. Introduction

Extraction and injection of fluids within petroleum reservoirs alters the ambient pore pressure leading to changes in the effective stress field within the reservoir and surrounding rocks. From the perspective of seismic monitoring, changes in the stress field can lead to nonlinear changes in seismic velocity observable in time-lapse seismic data (e.g. Barkved et al.[1], Herwanger and Horne[2], Barkved and Kristiansen[3], Kristiansen et al.[4]). However, changes in pore pressure do not necessarily lead to a hydrostatic change in effective stress. For instance, a reduction in fluid pressure within a reservoir is often accompanied by a slower increase of the minimum effective horizontal stress with respect to the vertical effective stress change (e.g. Hillis[5]). This asymmetry can result in the development of stress anisotropy that may promote failure within the rock, such as fault reactivation and casing deformation. This has important implications on the interpretation of time-lapse seismic as well as microseismic data, where stress anisotropy can result in anisotropic perturbations in the velocity field (e.g. Herwanger and Horne[6]) leading to induced seismic anisotropy, offset and azimuthal variations in reflection amplitudes, shear-wave splitting, and microseismicity if the stress exceeds the strength of the rock mass.

Over the past several decades, significant advances have been made in monitoring and predicting changes in physical properties within the subsurface related to petroleum production (e.g. Calvert[7], Fjær and Kristiansen[8], Johnson[9]). Yet uniquely relating surface deformation and time-lapse seismic observations to changes in rock physical properties is challenging (e.g. Herwanger et al.[10]). Recent improvements in the integration of coupled fluid-flow and geomechanical (or hydro-mechanical) simulation with rock physics and seismic modelling have led to a better understanding of changes in the physical properties of the subsurface and their time-lapse seismic signature (e.g. Olden et al.[11], Minkoff et al.[12], Herwanger and Horne[2,6]; Angus et al.[13], Trudeng et al.[14], He et al.[15]). Time-lapse seismic attributes have non-unique interpretations; for instance, observed changes could be due to changes in fluid saturation or to changes in the rock fabric itself (e.g., compaction). Hydro-mechanical modelling combined with seismic measurement and interpretation have the potential to help distinguish between these effects, and hence improve drilling[16] and completion practices, and identify areas where more production can be achieved. If successful, this would help reduce both the costs of conventional and unconventional production by reducing the number of wells necessary to achieve production targets.

In this paper, we integrate geomechanical, fluid-flow and seismic modelling to simulate the stress evolution during production to predict surface deformation and seismic attributes. A finite-element geomechanical simulator (ELFEN) is coupled to a reservoir fluid production simulator (VIP), where the output from the hydro-mechanical simulation is used to model surface subsidence, the seismic attribute AVOA (reflection amplitude versus offset and azimuth), and reservoir and overburden microseismicity. The integrated hydro-mechanical and seismic modelling workflow is applied to the data-rich Valhall oil reservoir in the southern part of the Norwegian sector of the North Sea. The field produces from relatively weak chalk in the Tor and Hod formations of Late Cretaceous age at a depth of about 2400 m. The field likely began deforming elastically, but over time transitioned to plastic deformation in some regions in the form of reservoir compaction, and this accelerated due to water weakening from pressure support. Hence Valhall has presented numerous geomechanical difficulties during its production lifespan. We compared predicted subsidence, AVOA response and microseismicity with observations from field data.

2. Hydro-mechanical and seismic modelling

Recent studies linking numerical coupled fluid-flow and geomechanical simulation with seismic modelling have improved our understanding of the relationship between seismic attributes, fluid properties and mechanical deformation due to reservoir fluid extraction and injection (e.g. Rutqvist et al.[17], Dean et al.[18], Herwanger and Horne[6], Alassi et al.[19], Angus et al.[20], Herwanger et al.[10], Schoenball et al.[21], Verdon et al.[22]). Analytic and semi-analytic approaches using poroelastic formulations for simple geometries have been used previously to understand surface subsidence (e.g. Geertsma[23]), microseismicity (e.g. Segall[24]) and seismic travel-time shifts (e.g. Fjær and Kristiansen[8], Fuck and Tsvankin[25], Fuck et al.[26]) due to pore pressure changes. Within the past decade, there has been significant effort to develop coupled fluid-flow and geomechanical numerical simulators primarily because they can be applied to more realistic geometries (e.g. Rutqvist et al.[17], Dean et al.[18], Minkoff et al.[27], Herwanger and Horne[6], Segura et al.[28]). Numerical hydro-mechanical simulators can integrate the influence of multi-phase fluid-flow as well as deviatoric stress and strain to provide more accurate models of the spatial and temporal behaviour of various rock properties within and outside the reservoir (e.g. Herwanger et al.[10]). Linking changes in reservoir physical properties, such as porosity, permeability and bulk modulus, to changes in seismic attributes is accomplished

via rock physics models (e.g. Prioul et al.[29]) to generate so-called dynamic (high strain rate and low strain magnitude suitable for seismic frequencies) elastic models.

2.1. Hydro-mechanical modelling

Coupling method: Industry standard fluid-flow simulators solve the equations of flow for multi-phase fluids (e.g. Aziz and Settari[30]), but tend to neglect the influence of changing pore pressure on the geomechanical behaviour of the reservoir and surrounding rock, when processes such as stress arching are active.[27,28] There are a considerable number of published papers related to the importance and applicability of coupled reservoir fluid-flow and geomechanical modelling. For example, Gutierrez and Lewis[31] show that compaction drive is not only dependent on the compressibility of the reservoir, but also the downward movement of the overburden, which cannot be properly accounted for without performing a coupled simulation. Dean et al.[18] show that the merit of explicit or coupled simulation is dependent on reservoir compaction scenario and the compressibility of the pay and non-pay formations. Formulations exist for fully coupled fluid-flow and geomechanical simulation, yet they tend to be computationally expensive (e.g. Minkoff et al.[27]) and often limited to single-phase flow. Iterative and loosely coupling fluid-flow simulators with geomechanical simulators can be computationally more efficient, yet yield sufficiently accurate results compared to fully coupled solutions (e.g.[18], Minkoff et al.[27]). Furthermore, iterative and loosely coupled approaches allow the use of already existing commercial reservoir fluid-flow and geomechanical modelling software. The coupling scheme employed in this paper is a staggered (incremental) external coupling method (see Fig. 1).

Constitutive model: Predicting the geomechanical response of reservoirs depends on the ability of the geomechanical simulator to model the nonlinear behaviour of rocks. The nonlinear dependence of rocks with stress is generally attributed to the deformation of microcracks and pores, grain-boundary contacts, and fractures with changing confining stress (e.g. Rutqvist[32], Herwanger and Horne[6]). Rock properties also display stress hysteresis (e.g. Helbig and Rasolofosaon[33], Hueckel et al.[34], Ferronato et al.[35]) and this hysteresis has been observed to occur not only at large strains but also small strains.[36] Hysteresis represents a potentially important rock characteristic in explaining the asymmetric behaviour of 4D seismic observations of producing reservoirs.[37] In this paper, the constitutive relationship used by the geomechanical simulator is the so-called SR3 (Soft Rock 3) model (see Appendix A.1) and is derived from laboratory experiments that incorporate linear poro-elastic and poro-plastic behaviour (e.g. Crook et al.[38]) as well as lithology specific deformation (e.g. Crook et al.[39]), where the model can be applied to various rock types such as sandstone, shale and chalk. For more details on coupling procedures between the geomechanical simulator and reservoir simulator see Angus et al.[40] and Segura et al.[28] An analysis of when coupling is needed is provided in Segura et al.[28] An additional feature of the SR3 model used for the Valhall simulation was the addition of chalk water weakening, where the yield surface properties are dependent on the change in water saturation compared to a reference state.

2.2. Integrated seismic modelling

Rock physics model: To model the seismic response due to geomechanical deformation, rock physics models are required to link changes in fluid saturation, pore pressure and triaxial stresses to changes in the dynamic elastic stiffness. These models should incorporate phenomena observed in both laboratory core experiments and in the field, such as the non-linear stress–velocity response (e.g. Nur and Simmons[41], Sayers[42], Hatchell and Bourne[37]) and the development of stress-induced anisotropy in initially isotropic rocks.[43,44,8] The nonlinear rock physics model is generally incorporated within an aggregate elastic model (see Angus et al.[40]). The approach has the benefit of allowing us to incorporate phenomena that act on multiple length-scales. Intrinsic anisotropy, caused by alignment of anisotropic minerals (such as clays and micas), can be included using an anisotropic background elasticity that can be constrained by laboratory methods (e.g. Valcke et al.[45], Kendall et al.[46]). Stress-induced seismic anisotropy, due to anisotropic changes in the effective stress field, is incorporated implicitly within the non-linear rock physics model. In other words, where there is a larger change in effective stress in one direction compared to another, the behaviour of the microcracks will vary in these directions leading to anisotropic changes in seismic velocity. Finally the influence of larger-scale sub-seismic fracture sets can also be modelled using the Schoenberg and Sayers[47] effective medium approach, adding the additional compliance of the larger fracture sets to the stress-sensitive compliance. Fluid substitution can also be included using either the Brown and Korringa[48] anisotropic extension to Gassmann's equation, which is appropriate as a low-frequency end member, or incorporating the dispersive effects of squirt-flow between pores.[49]

In this paper, we focus solely on the effects of nonlinear stress dependence of seismic velocities and assume that the rock has no intrinsic anisotropy or effective anisotropy due to the presence of coherent large-scale fracture sets. This is an entirely reasonable assumption given the weak nature of the reservoir and overburden. Several approaches have been developed to account for the influence of changes in stress and development of strain on seismic velocities, such as the one-dimensional vertical strain model,[37] the third-order elasticity theory model,[29,6] and the microcrack excess compliance model.[42,50,51] Angus et al.[52,13] use ultrasonic core data to calibrate the microcrack model of Verdon et al.[51] and observe that the rock physics input parameters have relatively consistent values that are specific to lithology (see Appendix A.2). Estimates of microcrack initial aspect ratio for most lithologies have mean of 0.0005, but differ for shale by up to an order of magnitude with mean of 0.001. Estimates of initial crack density are more diffuse, and are believed to be sensitive to core damage, microcrack/grain-boundary geometry and diagenesis. Based on the results of the calibration

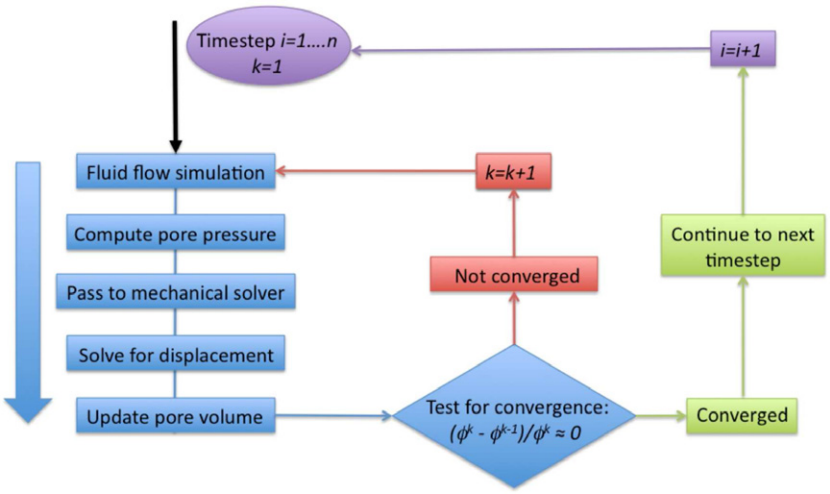

Fig. 1. Diagram showing the iterative coupling between the fluid flow and geomechanical simulators. At each time step the flow simulator computes the pore pressure and fluid properties, which are subsequently passed to the geomechanical simulator to compute deformation. The geomechanical simulator computes changes in porosity, which is returned to the flow simulator to recomputed pore pressures using the updated pore volumes. This iterative process, passing pore pressures and pore volumes between the mechanical and flow simulators, is iterated until a stable value for porosity (and a corresponding value for pore pressure) is reached, at which point the simulation moves to the subsequent time-step.

Table 1
Mechanical properties for the 30-layer Valhall model, where E is Young's modulus, ν is Poisson's ratio, G is shear modulus, and □ is porosity (properties of the overburden and reservoir were published in Kristiansen and Plischke[53] and based on the work of Wittke (1990)). Orthotropic anisotropy (or vertical transverse isotropy) is incorporated, where the Cartesian coordinates are defined with z being depth and x, y being lateral coordinates. The overburden (layers 1–11) is modelled as an orthotropic linear elastic material. The reservoir sections (layers 12–24) are modelled as an isotropic poro-elasto-plastic material. The upper section of the under-burden (layers 26 and 27) is modelled using a linear elastic material behaviour, whereas the lower section (layers 28–30) is modelled using an orthotropic linear elastic material behaviour.

	Layer		$E_x : E_y$ E_1	E_z E_2	ν_{xy} ν_1	$\nu_{xz} : \nu_{yz}$ ν_2	G_{xy} G_1	$G_{xz} : G_{yz}$ G_2	ε_i	a_o ($x10^4$)
	1	T200	240	150	0.25	0.15	96	55		
	2	T180	300	180	0.25	0.15	120	66		
	3	Intra mid Miocene	400	240	0.25	0.15	160	88	0.250	1
	4	T110	500	300	0.25	0.15	200	110	0.245	1
	5	Intra late Oligocene	650	390	0.25	0.15	260	130	0.240	1
Overburden	6	Intra late Eocene	700	420	0.25	0.15	280	154	0.238	1
	7	Early Eocene	750	450	0.25	0.15	300	165	0.238	1
	8	–	=	=	=	=	=	=	=	=
	9	Balder	2000	600	0.25	0.10	800	200	0.197	1
	10	Sele	1100	900	0.30	0.20	423	360	0.227	1
	11	Lista	1200	1000	0.30	0.20	461	360	0.224	1
Reservoir & Side-burden	12 to 19 20 to 24	Tor Hod	$E = 1000\phi^{-1.1}$		0.175		X		0.230	10
	26 to 27	Chalk	7000		0.170		X		0.033	1
Under-burden	28 to 29	Shale	7000	4000	0.20	0.10	2917	1500	0.033	1
	30	Shale	8000	6000	0.20	0.10	3333	2500	0.033	1
Faults	31 to 60	Reservoir	$E = 900\phi^{-1.1}$		0.25		X		0.230	1
	61 to 90	Overburden	300		0.30		x		0.005	1

studies,[52,13] we use the scalar microcrack analytic model as it yields a reasonably accurate prediction of the nonlinear stress dependence of seismic velocities and anisotropy. Table 1 shows the layer specific values used for the model initial crack density and initial aspect ratio.

AVOA prediction: In AVOA analysis, multi-offset and multi-azimuth reflection amplitude data are reduced to a set of parameters, such as the normal incidence amplitude and the principal AVO gradients. Generally only short-offset data are considered, where the variation in reflection amplitudes with azimuth (ϕ) can be described by a simple $\cos 2\phi$ trend (e.g. Ruger[54]). Hall and Kendall[55] calculate AVOA parameters in three key stages. First, a three-term AVO curve is calculated using data in overlapping 25 m × 25 m common midpoint bins. Second, the normal-incidence amplitude term is used to evaluate the azimuthal dependent near-offset AVO gradient term. Finally, the AVOA algorithm assumes the near-offset AVO gradient is elliptical allowing the orientation and magnitude of anisotropy to be determined from the AVO coefficients. Although the AVOA observations of Hall and Kendall[55] are a measure of the near-offset AVO gradient and not

velocity anisotropy, the method provides a measure of fracture orientation and strength. Velocity anisotropy can be estimated using an effective fractured medium rock physics model (e.g. Hall[56]).

To predict the AVOA response, we calculate the complex valued reflection coefficients using an anisotropic layer-matrix approach (e.g., see Angus and Thomson[57] for description of the theory). The reflection coefficient of any interface between two layers is evaluated using the elasticity tensor of the upper and lower layers. For the Valhall model, the algorithm provides synthetic amplitudes at specified offsets and azimuths for each grid point within the hydro-mechanical seismic sub-volume and for each chosen horizon. The predicted AVOA response will be sensitive to the geometry of the model as well as the stress-dependence of the nonlinear microcrack rock physics transform (see Appendix B).

Microseismic model: An important observable manifestation of geomechanical deformation is brittle failure, which can be linked to microseismic activity. Regions that have high shear stress have an increased risk of brittle failure, implying higher microseismicity rates. If mechanical simulations include brittle and plastic behaviour in their constitutive models, then regions of high shear stress or matrix failure can be used as direct indicators of microseismic activity. There remains a degree of uncertainty regarding the best method of predicting microseismic activity based on finite-element geomechanical models.

We have developed two parallel methods to predict microseismicity on reservoir field scale using finite-element hydro-mechanical simulations. The first approach is applied to poroelastic simulations and considers the evolution of deviatoric stress with respect to the Mohr–Coulomb failure envelope. This can be formalized using the fracture potential term (e.g. Verdon et al.[22]), which describes the ratio of the in-situ deviatoric stress to the critical stress required for failure on an optimally oriented surface. A higher value for fracture potential corresponds to a higher risk of microseismicity for the node in question. The second approach is applied to poroelastoplastic simulations and involves tracking matrix failure during the geomechanical simulation[20]. This microseismic modelling method allows for a continuous prediction of the temporal and spatial distribution of seismicity. In this approach, the geomechanical simulator internally tracks regions undergoing yield and for each failure event, the stress tensor, pore pressure and elastic tensor are recorded. In this study, the matrix failure approach to microseismic prediction is used to provide an estimate (i) of regions within the model that might generate seismicity, and (ii) direction and type of the failure (tensile, shear or shear-enhanced compaction).

3. Valhall model

The Valhall reservoir is a large chalk field with well-preserved porosity of up to 50% in certain parts of the field. The high porosity is due to the highly over-pressured reservoir units and, as such, compaction provides the main drive mechanism for production. Compaction also plays a critical role in field geomechanics: total subsidence currently exceeds 6 m below the central platforms. The Valhall hydro-mechanical model was developed and implemented to predict future subsidence, assist drilling and optimize casing designs in the highly depleted and compacted crest of Valhall field (see Table 1 for mechanical properties). Due to the maturity of this field, the reservoir fluid-flow simulation models have been extensively history-matched with production data and, three-dimensional full-field finite-element based geomechanics model for overburden and reservoir has been history-matched with production data (e.g. Kristiansen and Plischke[53]). In this paper, the hydro-mechanical simulations for Valhall involved coupling the ELFEN geomechanical simulator (Rockfield Software Ltd) with the reservoir flow simulator VIP (Halliburton). The finite-element mesh was created using the grid generator RMS/TEMPEST (Roxar Ltd) and consists of 30 layers created from the geological model. The geomechanical mesh begins from the sea floor, but it includes the water column loading. The ELFEN geomechanical simulation was performed using a tetrahedral mesh of approximately 6 million finite elements and the VIP simulation was performed using a finite-difference mesh of 0.5 million cells (see Fig. 2). Since the ELFEN and VIP mesh are different, parameters between meshes are transferred during the coupling stage using a spatial mapping algorithm based on the least-squares method. The hydro-mechanical model has been constrained by a range of field and surveillance data: GPS, time-lapse seafloor bathymetry,[53] radioactive markers in reservoir and overburden, and time-lapse seismic.

The geomechanical model was initialized using in-situ geostatic stresses to establish the pre-production status of the Valhall field. Specifically, the background geostatic stresses were applied via a 1-D geostatic stress profile under the following conditions: (a) the vertical total stresses are based on the gravitational forces and material bulk density, and are maintained by the application of gravitational acceleration g; (b) the pore pressure is assumed to be hydrostatic with over-pressure if applicable (i.e. modelled according to measurements and predictions of overpressure), and (c) horizontal effective stresses are assigned based on the assigned k_0 ratios (ratio of vertical to lateral earth pressures) and the calculated vertical effective stress or from initial fracture pressure measurements where available. The values of $k_0 = 0.75$ and $k_0 = 0.5$ were used for the Tor and Hod reservoirs, respectively.[58,53] Following initialization, the hydro-mechanical response due to production was simulated using a two-way coupling scheme, where the geomechanical model used the pore pressure evolution calculated in the reservoir simulator and the reservoir simulator used the updated pore volume change calculated in the geomechanical simulator. For the over-, under- and side-burden, the pore pressure was kept constant during the simulation in these cases.

To map the hydro-mechanical results to seismic velocities, we used average microcrack parameters inverted using chalk and shale core data (see Angus et al.[52]). The chalk data used in Angus et al.[52] is consistent with that present by Alam et al.[59] For the reservoir rocks, we used an initial crack density and initial aspect ratio of 0.25 and 0.0001, respectively. For the non-reservoir rocks we used an initial crack density and initial aspect ratio of 0.125 and 0.001. For this preliminary work, we did not have sufficient rock

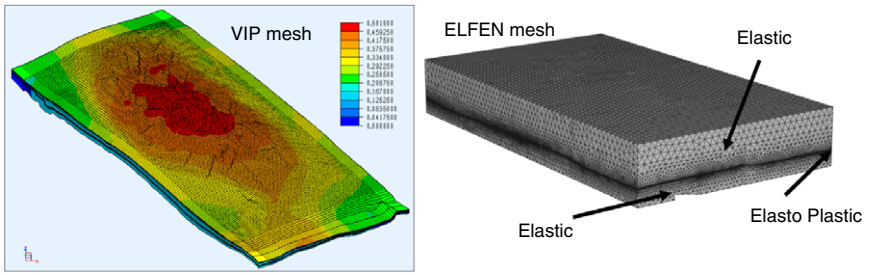

Fig. 2. Left: VIP reservoir flow model defined by finite-difference mesh consisting of 0.5 million cells, having dimensions 19 km × 8 km laterally and 600 m in thickness. The colour contours represent reservoir porosity, ranging from 0.0 (blue) to 0.5 (red). Right: ELFEN geomechanical model for Valhall consisting of 6 million tetrahedral finite-elements, having lateral extent of 16 km × 28 km and depth extent of 4.2 km. The reservoir is located at 2500 m depth (as shown by the dense layer of finite-elements). (For interpretation of the references to colour in this figure legend, the reader is referred to the web version of this article.)

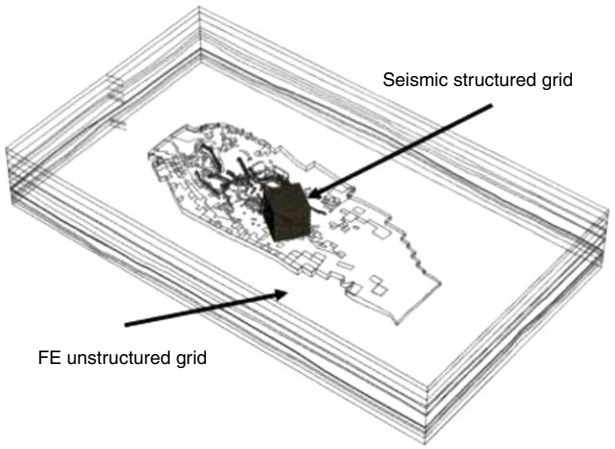

Fig. 3. Location of the seismic grid sub-volume within the finite-element geomechanical mesh. The seismic grid has dimensions 2 km × 2 km laterally and 3.5 km in depth. The discrete grid consists of 50 × 50 lateral cells (lateral grid increment of 40 m) and 150 cells vertically (depth increment of 20 m).

data to justify using depth-dependent or anisotropic initial microcrack properties. However, even with isotropic initial microcrack parameters, the rock physics model allows seismic anisotropy to develop due to non-hydrostatic stress change (see Verdon et al.[51]). For the AVOA predictions, we selected a sub-volume of the field (the south-east section of the crestal area), where previously published 4D seismic anisotropy studies are available (e.g. Hall and Kendall[55]). Fig. 3 shows the sub-volume with respect to finite-element model.

4. Results

The hydro-mechanical simulation is performed for both one-way and two-way coupling. In the one-way coupling, pore pressures from the flow simulator are passed to the geomechanical simulator and the reservoir flow simulator uses a table of pore volume multipliers. The table is then used to update porosity within the flow simulation based on geomechanically predicted pressure changes. In the two-way coupling, hydro-mechanical simulation is driven by exchanging information between the reservoir flow simulator and the geomechanical simulator: pore pressure and water saturation calculated in the reservoir simulator are passed to the geomechanical simulator, the geomechanical simulator updates the pore volume and passes this update back to the flow simulator. In both coupling cases, the hydro-mechanical solution accounts to varying degrees of accuracy for the strain rate dependent reservoir compaction during depletion, re-pressurization and water flooding. In this study, no effort was made to history-match the two-way coupled model since this is a time consuming and more challenging task than history-matching a one-way coupled model. However, time-lapse seismic and microseismic data are another potential source of data that can be used to improve geomechanical model calibration as well as improve two-way coupling by minimizing misfit between prediction and observation.

4.1. Subsidence

Fig. 4 compares the results of surface subsidence prediction using the one-way coupling and the field measurement. The results show very good match with the observed data for the evolution of vertical displacement predictions below the QP North and South platforms during approximately 25 years production is shown.

4.2. AVOA

There have been several studies of azimuthal seismic anisotropy carried out for the Valhall reservoir using the

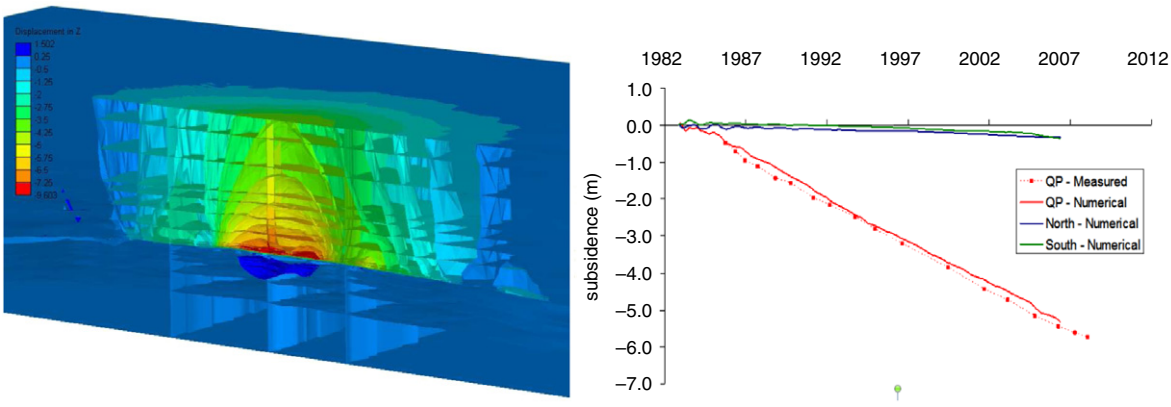

Fig. 4. Left: Vertical section through the Valhall model showing the predicted vertical displacement isosurfaces, ranging from +1.5 (blue) to −9.0 (red). Right: Evolution of vertical displacement predictions of the sea floor surface below the QP platforms. GPS subsidence measurements are only available for the QP platform and not the North and South flank platforms. (For interpretation of the references to colour in this figure legend, the reader is referred to the web version of this article.)

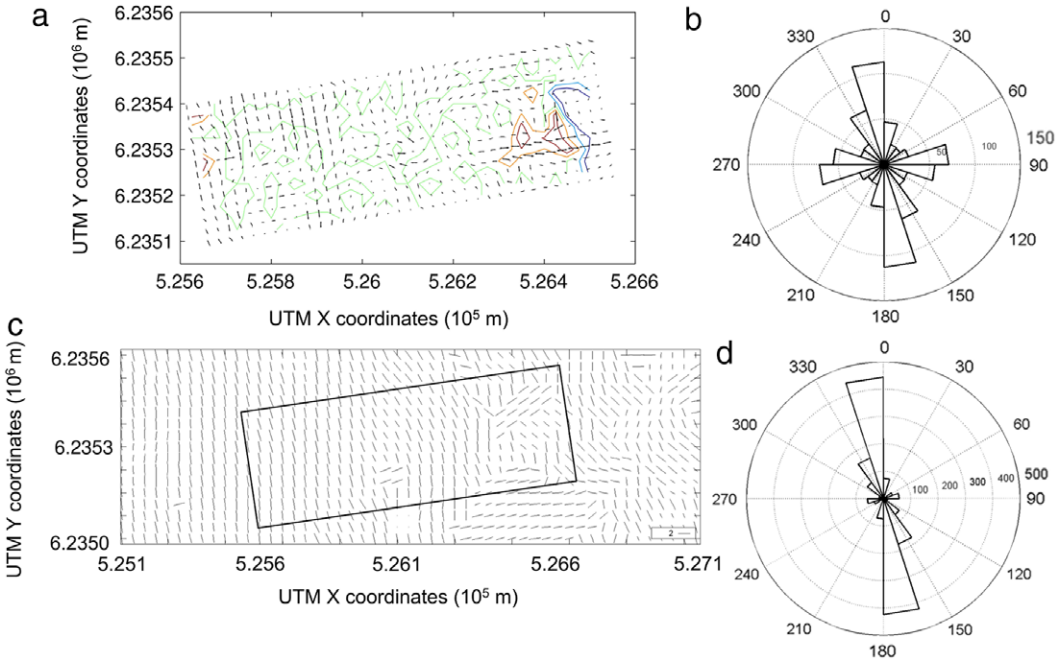

Fig. 5. Comparison of the observed[56] and predicted AVOA response at Valhall for the Base Miocene horizon: (a) observed AVOA pattern, (b) polar area diagram showing the dominant orientation of the AVOA anisotropy for the observed data, (c) predicted AVOA pattern (note the area within rectangle approximately corresponds to the observed data), and (d) polar area diagram showing the dominant orientation of the AVOA anisotropy for the predicted data.

multicomponent ocean bottom seismic (OBS) array.[60,55] The OBS array consisted of 4C cables with 600 m × 600 m cross-spread, providing good azimuthal distribution. Olofsson et al.[44] provided one of the earliest seismic anisotropy studies, examining the crestal zone using P-to-S mode conversions using data acquired in 1997–1998 with the 3D 4C OBS array. By performing shear-wave splitting analysis of the mode conversions using a layer stripping method, Olofsson et al.[44] observed radial anisotropy in the near surface consistent with the subsidence bowl as well as anisotropy patterns related to subsurface structure and fracture systems. Using the same data, Hall and Kendall[55] performed AVOA analysis on the southeast section of the anticlinal structure and observed AVOA patterns consistent with fracture distributions and faults within the reservoir. The length-scales of the fractures are sub-seismic wavelengths,[55] and so could be due to not only sub-seismic scale fractures but also microcracks. However, recent analysis suggests that the AVOA pattern is sensitive also to lithology and geometry, where some of the shear fractures act as baffles to fluid-flow.[61]

Figs. 5–7 compare the predicted AVOA seismic response for a sub-volume of the field to the previous published AVOA seismic results of Hall.[56] In Fig. 5, the AVOA patterns

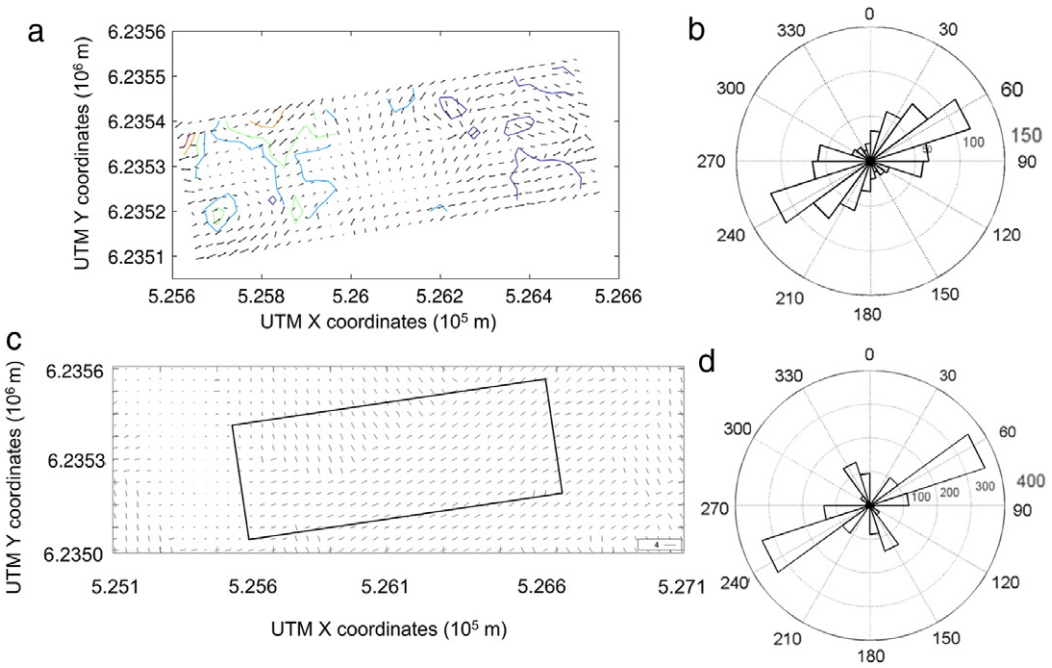

Fig. 6. Comparison of the observed[56] and predicted AVOA response at Valhall for the 2130 ms horizon (see Fig. 5 for details).

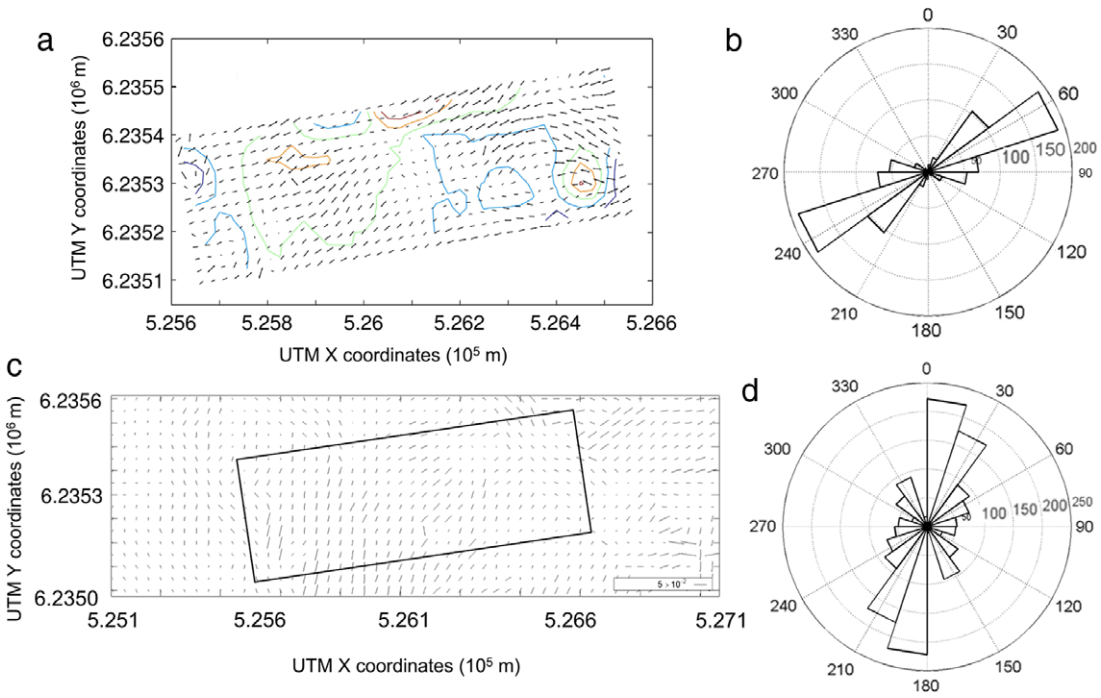

Fig. 7. Comparison of the observed[56] and predicted AVOA response at Valhall for the Top Chalk horizon (see Fig. 5 for details). Although the azimuthal pattern of anisotropy is a poor fit, the relative magnitude of anisotropy is more consistent.

for the Base Miocene horizon show some consistency, with predominant anisotropy oriented North–South. However, there is also significant anisotropy oriented East–West in the observed data that is not predicted in the model. The results for the 2130 ms horizon are shown in Fig. 6. The patterns also show some similarity, with predominant anisotropy oriented approximately East–West. Both AVOA patterns show a wedge like pattern in the top-left quadrant, whereas the circular pattern in the observed data at UTM Y 6.2353 and UTM X 5.258 appears further to the left in the model prediction. In Fig. 7, the results for the Top Chalk horizon are shown, where there is weaker

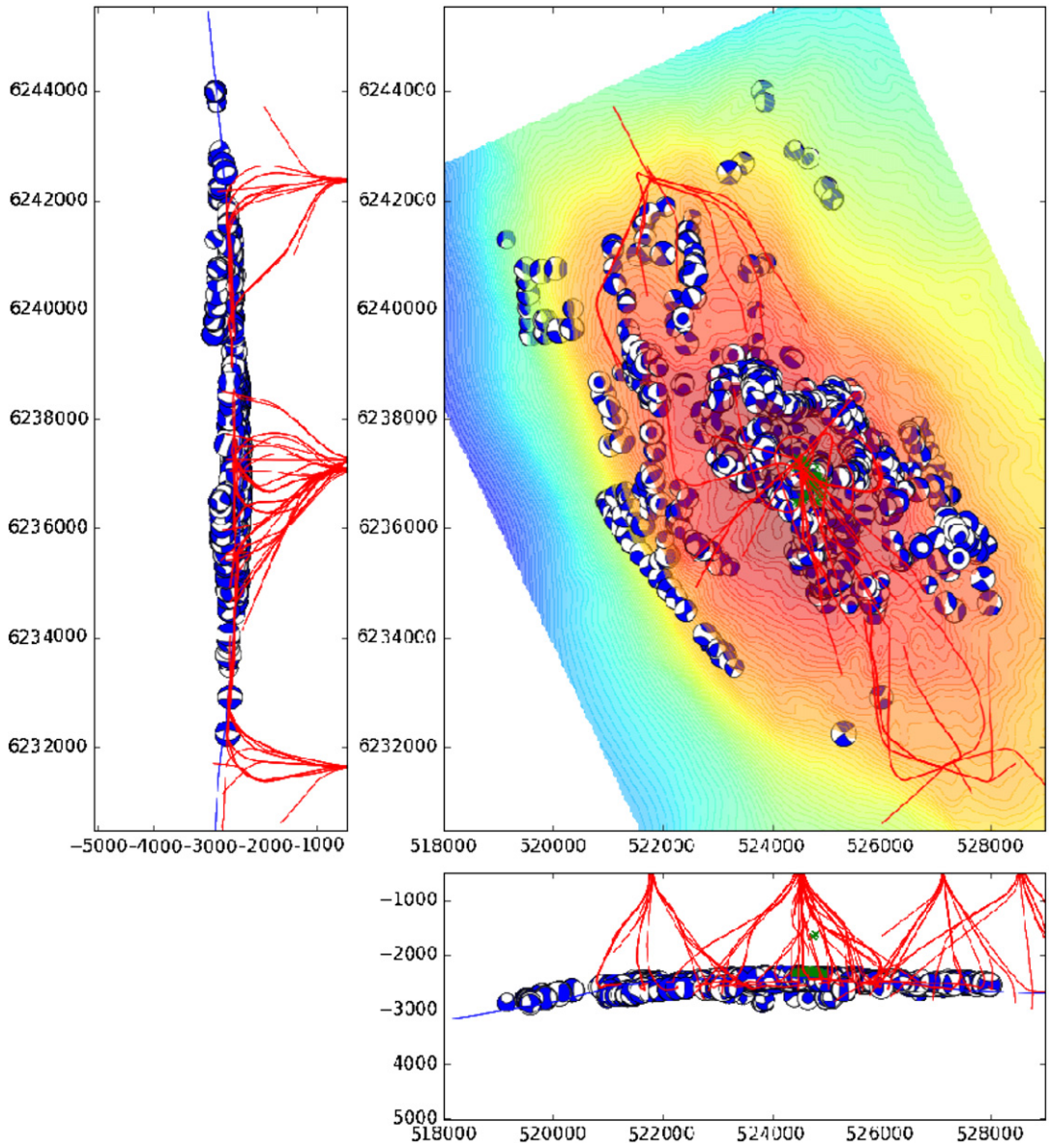

Fig. 8. Predicted shear-type microseismic events (focal solutions are plotted using Harvard CMT with zero trace) for the 25 years of production. The size of the focal sphere indicates the relative magnitude of the predicted event (see Angus et al.[20] for details of how the mechanisms and magnitudes are calculated). The top of the reservoir is shown by the blue surface (in the vertical sections) and as a contour (in map view) with red depicting the anticline structure. The green symbols are the location of the observed microseismic events[62] and the red lines represent the location of the wellbore trajectories. (For interpretation of the references to colour in this figure legend, the reader is referred to the web version of this article.)

similarity between the predicted and observed AVOA response. There are weak circular patterns occurring within the right side of the horizon. However, the orientation of dominant anisotropy shown in the polar plots are not in agreement, with the observed data being oriented approximately East–West and the model predictions oriented approximately North–South. It is encouraging that the initial model predictions compare broadly with the seismic observations of anisotropy for these two horizons considering that there was no calibration of the rock physics models to the Valhall data and that we did not include sub-seismic fractures within the geomechanical model.

4.3. Microseismicity

We use the matrix failure approach of Angus et al.[20] to predict microseismicity from the hydro-mechanical simulation. A limit on the number of elements used in the finite-element based geomechanical simulator means that the microseismic predictions are limited by the continuum formulation (i.e., not localized). Although this approach cannot model the micro-mechanical behaviour as can be done with discrete-element and particle-flow geomechanical solutions, it does provide a first-order estimate of regions within the model that might generate

seismicity and potentially the type of failure (tensile, shear or shear-enhanced compaction). It is important to note that it is unlikely that tensile or shear-enhanced compaction type events would be observable within reservoirs given the distance between the event locations and the geophones, whereas shear-type events would be as they generate much larger seismic energy. For realistic model geometries, proper geostatic initialization and sufficiently accurate hydro-mechanical history matching using well data, continuum based finite-element simulators should provide reasonable prediction of the stress and strain evolution. As was seen in Fig. 4, the accurate subsidence predictions suggest that the evolution of strain within the model is not only globally reasonable but also locally on the scale of the finite-element meshes. Since the Valhall model includes mechanical anisotropy and subsurface structure, the microseismic predictions should represent plausible first-order predictions of seismicity and their average mechanisms.

In Fig. 8, the distribution of all shear-type microseismic events for the complete finite-element mesh is shown (i.e., microseismic predictions are done for the whole hydro-mechanical model and not limited to the seismic sub-volume). The lateral distribution of events follows a north-west/south-east distribution consistent with the results of Zoback and Zinke[62] and follows the long-axis of the anticlinal reservoir structure. The shear-type events are primarily localized between 2300 and 3000 m depth within the lower Balder formation. Dyer et al.[63] examine microseismic data and observe depth distribution of events between 2300 and 2400 m, which is consistent with our predictions for the sub-volume that they examine.

In Fig. 9, the predicted moment tensor mechanisms are plotted using the geometrical representation of Tape and Tape[64]. The predicted shear-type solutions fall within plausible mechanisms, with many events being predominantly double-couple failure as well as both positive and negative linear vector dipole failure indicative of volumetric components. The predicted double-couple mechanisms are predominantly normal fault type, which is consistent with the composite double-couple solution of Zoback and Zinke.[62]

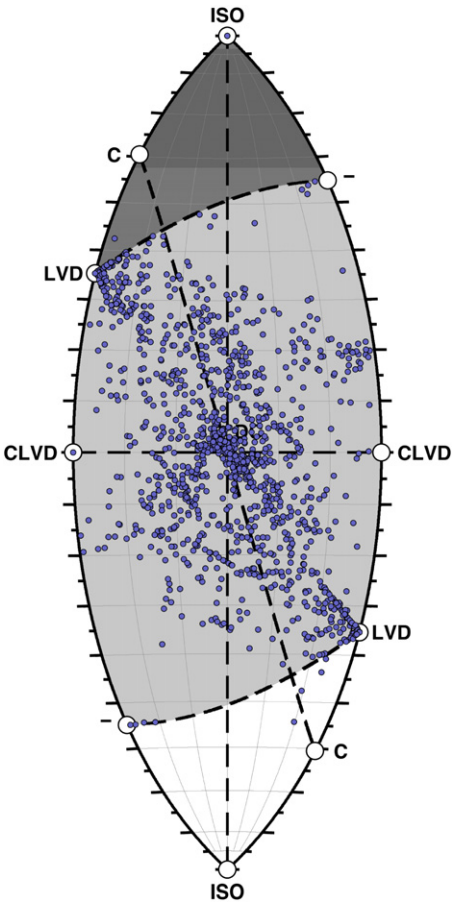

Fig. 9. Predicted shear-type mechanism of the moment tensor solutions are plotted and are consistent with other observed reservoir microseismic mechanisms.[64] In this figure, ISO represents explosive (top dark grey shaded region) and implosive (bottom white shaded region) failure, LVD represents linear vector dipole failure, CLVD represents compensated linear vector dipole failure, and C represents crack (tensile crack) failure. Double-couple shear failure is located in the centre of the figure at the intersection of the horizontal line joining the CLVD mechanisms and the vertical line joining the ISO mechanisms. All the shear-type events fall within the region of expected shear type failure (light grey shaded region).

5. Conclusions

The integrated geomechanical, fluid-flow and seismic modelling workflow has shown promise in predicting several manifestations of geomechanical deformation. The results of the surface subsidence predictions compare very well with field observations. Using a non-linear rock physics model calibrated with core data, the predicted AVOA response closely resembles that measured from field seismic data. This result is very encouraging given that there was no further calibration of the rock physics model to Valhall specific core data or the Valhall hydro-mechanical simulation. The spatial pattern of modelled microseismicity is consistent with previously published microseismic analyses and the modelled failure mechanisms are consistent with typical reservoir induced seismicity (e.g., predominantly double couple failure with variable volumetric component). The results of this study suggest that seismic data can be used to improve hydro-mechanical model calibration, which can be significant since seismic data provide greater control over a much larger volume of the hydro-mechanical model. Furthermore, integrated seismic and hydro-mechanical model can improve the non-uniqueness of time-lapse seismic interpretation, for instance leading to identification of reservoir volumes for infill drilling and also predicting stress changes for optimizing hydraulic fracturing. The next steps involve using seismic data to calibrate hydro-mechanical models, such as uncertainty in rock physics models (e.g., intrinsic anisotropy, static-to-dynamic elastic conversion, calibration of input model parameters and in-situ stress sensitivity). As well, temporal variations in shear-wave anisotropy[65] and multiplet behaviour of fault failure De Meersman et al.[66] from microseismic data could be used to further constrain the hydro-mechanical models.

Acknowledgements

The authors would like to thank the sponsors of the ITF joint-industry projects IPEGG (BG, BP, ENI and Statoil) and GESER (Shell, ConocoPhillips, Chevron and DECC). The authors thank Rockfield Software for access to the geomechanical simulator ELFEN, and Roxar for access to the geological model builder RMS (TEMPEST), and Halliburton for access to VIP. The Valhall license (BP Norge AS and Hess Norge AS) is thanked for permission to publish this research.

Appendix A. Constitutive and rock physics models

A.1. Constitutive model

We have adapted the existing ELFEN Soft Rock 3 constitutive (SR3) model[38,39] to predict liquefaction of chalk.[67] The SR3 model is a Cam-Clay type of model, which is strain rate dependent and so it takes into account time dependent deformations, or creep. An additional feature within the SR3 model was developed for Valhall allowing for water weakening within the Chalk. This feature was developed in a way so that the yield surface properties are dependent on the change in water saturation compared to a reference state. Fig. A.1 shows examples of data from laboratory water-flood experiments on Valhall chalk as well as the prediction of the water weakening response based on the model developed in ELFEN. The results are very good and acceptable for prediction in a full field model.

Young's modulus has the following dependency

$$E = 46e^{-8.25\,\emptyset_{INI}},$$

where ϕ_{INI} represents the initial porosity and is in units of GPa. This dependency describes the deformation of the rock mass and reflects the influence of fractures, local porosity variation and heterogeneity, and as such is smaller than moduli measured from intact core samples. More details on the material properties are provided in Kristiansen and Plischke.[53]

A.2. Rock physics model

To enable forward modelling of time-lapse seismic effects related to perturbations in stresses, Verdon et al.[51] extended the analytic effective medium formulation of Tod[68] to predict ultrasonic anisotropic and stress-dependent velocities. Specifically, the analytic microcrack model introduces initial microcrack aspect ratio and number crack density to predict stress dependence and crack-induced elastic anisotropy. The number crack density is written

$$\epsilon_i\left(\sigma_{ii}^e\right) = \epsilon_i^o e^{-c_r\sigma_{ii}^e},$$

where

$$c_r = \frac{1}{\pi\,\mu_i \mathrm{a}_i^o}\left(\frac{\lambda_i + 2\mu_i}{\lambda_i + \mu_i}\right)$$

ϵ_i^o and a_i^o are the effective initial number crack density and effective initial aspect ratio, λ_i and μ_i are the Lame constants, and σ_{ii}^e is the principal effective stress in the ith direction. The second-rank microcrack density term is

$$a_{ii} = \frac{\epsilon_i}{h_i},$$

where

$$h_i = \frac{3E_i^o}{32}\left(\frac{2-\nu_i^o}{1-\left(\nu_i^o\right)^2}\right)$$

is a normalization factor,[69] and E_i^o and ν_i^o are the anisotropic intact rock Young's modulus and Poisson ratio. This derivation yields an expression for the effective elasticity that can model stress-induced elastic anisotropy due to deviatoric stress fields. The key assumptions for this model are that the microcracks are penny-shaped and that the rock does not undergo brittle or plastic deformation. Using the approach of Sayers and Kachanov[70] and Schoenberg and Sayers[47], the excess compliance $\Delta\boldsymbol{S}$ (the inverse of the $3\times3\times3\times3$ elasticity tensor $\boldsymbol{C}$) due to the deformation of microcracks is used to compute the stress dependence and induced elastic anisotropy

$$\Delta S_{ijkl} = \frac{1}{4}\left(\delta_{ik}a_{ji} + \delta_{jk}a_{il} + \delta_{il}a_{jk} + \delta_{jl}a_{ik}\right),$$

where δ_{ij} is the Kronecker delta and summation convention is being used.

Appendix B. AVOA

The seismic reflection P-wave amplitude variation with offset and azimuth (AVOA) technique was developed for detecting sub-seismic vertical fracture sets. The reflected seismic is influenced by the interaction of the incident seismic wave with a discontinuity in material properties (seismic velocity and/or density), where the energy of the incident wave can be converted into up to six secondary waves. Although Snell's law can be used to determine the directional properties of all the secondary waves, it cannot provide information on waveform amplitudes and pulse distortion. Thus a more complete evaluation of the reflection and transmission (R/T) properties is needed. The solution to the R/T response involves using a local plane-wave and plane-boundary approximation (see Angus and Thomson[57]). The AVOA technique utilizes the AVOA intercept (P-wave normal-incidence reflectivity $\boldsymbol{A}$) and two gradients: an azimuthally invariant isotropic component $\boldsymbol{G_{iso}}$ and an azimuthally dependent anisotropic contribution $\boldsymbol{G_{aniso}}$ (see Ruger[54], Jenner[71])

$$R_P^{HTI}(\theta,\gamma) = A + \left(\boldsymbol{G_{iso}} + \boldsymbol{G_{aniso}}\,(\cos\gamma)^{\mathbf{2}}\right)(\sin\theta)^2,$$

where

$$A = \frac{1}{2}\frac{\Delta Z}{Z}$$

$$\boldsymbol{G_{iso}} = \frac{1}{2}\left[\frac{\Delta a}{a} - \left(\frac{2\beta}{a}\right)^2\frac{\Delta G}{G}\right]$$

$$\boldsymbol{G_{aniso}} = \frac{1}{2}\left[\Delta\delta^{(V)} + 2\left(\frac{2\beta}{a}\right)^2\Delta\gamma\right].$$

In Figs. 6–8 we only plot the fast orientation of the anisotropy, which is orthogonal to the direction of maximum $\boldsymbol{G_{aniso}}$.

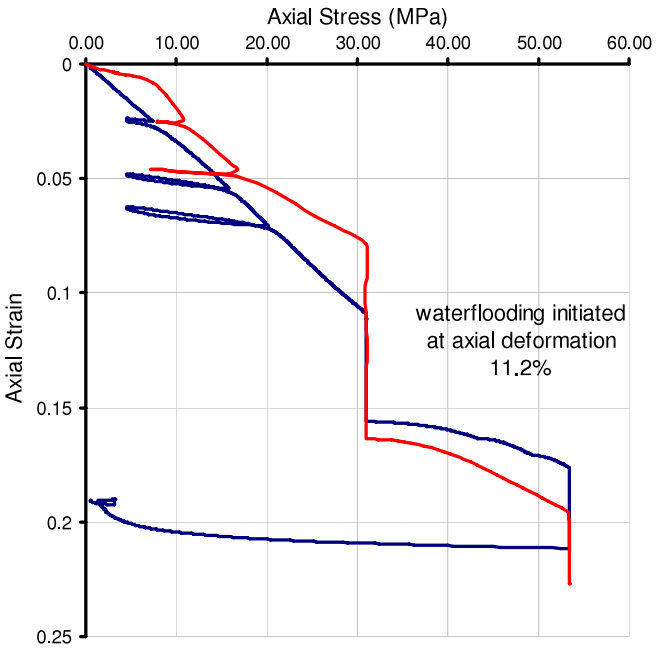

Fig. A.1. Comparison of laboratory tests showing loading/unloading cycles and water weakening of Valhall chalk and numerical modelling based on the extended SR3 model in ELFEN. The blue line is the experimental data and the red line is the modelled data. (For interpretation of the references to colour in this figure legend, the reader is referred to the web version of this article.)

References

[1] O Barkved, P Heavy, R Kjeldstadli, T Kleppan, TG Kristiansen, Valhall field — still on plateau after 20 years of production, SPE 83957; 2003.

[2] Herwanger JV, Horne SA. Predicting time-lapse stress effects in seismic data. *Lead. Edge* 2005;24:1234–1242.

[3] Barkved OI, Kristiansen T. Seismic time-lapse effects and stress changes: Examples from a compacting reservoir. *Lead. Edge* 2005; 1244–1248.

[4] TG Kristiansen, OI Barkved, K Buer, R Bakke, Production induced deformations outside the reservoir and their impact on 4D seisimic, In: International Petroleum Technology Conference, Doha, Qatar, 21–23 November, 2005, paper IPTC 10818.

[5] Hillis RR. Coupled changed in pore pressures and stress in oil fields and sedimentary basins. *Pet. Geosci.* 2001;7(4):419–425.

[6] Herwanger JV, Horne SA. Linking reservoir geomechanics and time-lapse seismics: Predicting anisotropic velocity changes and seismic attributes. *Geophysics* 2009;74(4):W13–W33.

[7] Calvert R. *Insights and Methods for 4D Reservoir Monitoring and Characterization*. Distinguished Instructor Series, No. 8. EAGE; 2005.

[8] E Fjær, TG Kristiansen, An integrated geomechanics, rock physics and seismic model, In: 71st EAGE Conference and Exhibition — Amsterdam, The Netherlands, 2009; June 2009:8–11.

[9] Johnson DH. *Practical Applications of Time-lapse Seismic Data*. Distinguished Instructor Series, No. 16. EAGE; 2013.

[10] Herwanger JV, Schitt CR, Frederiksen R, If F, Vejbk OV, Wold R, Hansen HJ, Palmer E, Koutsabeloulis N. Applying time-lapse seismic to reservoir management and field development planning at South Arne, Danish North Sea. *Petroleum Geology: From Mature Basins to New Frontiers, Proceedings of the 7th Petroleum Geology Conference*. In: Vining BA, Pickering SC, eds. 2010.

[11] Olden P, Corbett P, Westerman R, Somerville J, Koutsabeloulis N, Smart B. Modelling combined fluid and stress change effects in the seismic response of a producing hydrocarbon reservoir. *Lead. Edge* 2001;20:1154–1163.

[12] Minkoff SE, Stone CM, Bryant S, Peszynska M. Coupled geomechanics and flow simulation for time-lapse seismic modeling. *Geophysics* 2004;69(1):200–211.

[13] Angus DA, Fisher QJ, Verdon JP. Exploring trends in microcrack properties of sedimentary rocks: An audit of dry and water saturated sandstone core velocity-stress measurements. *Int. J. Geosci.* 2012;3: 822–833.

[14] T Trudeng, X Garcia-Teijeiro, A Rodrigues-Herrera, J Khazanehdari, Using stochastic seismic inversion as input for 3D geomechanical models, In: International Petroleum Technology Conference, 17547, 2014.

[15] He Y, Angus DA, Clark RA, Hildyard MW. Analysis of time-lapse travel-time and amplitude changes to assess reservoir compartmentalisation. *Geophys. Prospect.* 2015.

[16] TG Kristiansen, RE Flatebø, 60 days ahead of schedule-reducing drilling risk at valhall using computational geomechanics, In: SPE/IADC Drilling Conference and Exhibition, Amsterdam, The Netherlands, 17–19 March, 2009, paper SPE/IADC 119509.

[17] Rutqvist J, Wu Y-S, Tsang CF, Bodvarsson G. A modeling approach for analysis of coupled multiphase fluid flow heat transfer, and deformation in fractured porous rock. *Int. J. Rock Mech. Min. Sci.* 2002; 39:429–442.

[18] Dean RH, Gai X, Stone CM, Minkoff SE. *A Comparison of Techniques for Coupling Porous Flow and Geomechanics*. Society of Petroleum Engineers; 2003:79709.

[19] Alassi H, Holt R, Landro M. Relating 4D seismics to reservoir geomechanical changes using a discrete element approach. *Geophys. Prospect.* 2010;58:657–668.

[20] Angus DA, Kendall J-M, Fisher QJ, Segura JM, Skachkov S, Crook AJL, Dutko M. Modelling microseismicity of a producing reservoir from coupled fluid–flow and geomechanical simulation. *Geophys. Prospect.* 2010;58(5):901–914.

[21] Schoenball M, Muller TM, Muller BIR, Heidbach O. Fluid-induced microseismicity in pre-stressed rock masses. *Geophys. J. Int.* 2010; 180:813–819.

[22] Verdon JP, Kendall J-M, White DJ, Angus DA. Linking microseismic event observations with geomechanical models to minimise the risks of storing CO2 in geological formations. *Earth Planet. Sci. Lett.* 2011;305:143–152.

[23] Geertsma J. Land subsidence above compacting oil and gas reservoirs. *J. Pet. Geol.* 1973;25(6):734–744.

[24] Segall P. Earthquakes triggered by fluid extraction. *Geology* 1989;17: 942–946.

[25] Fuck RF, Tsvankin I. Analysis of the symmetry of a stressed medium using nonlinear elasticity. *Geophysics* 2009;74(5):WB79–WB87.

[26] Fuck RF, Tsvankin I, Bakulin A. Influence of background heterogeneity on traveltime shifts for compacting reservoirs. *Geophys. Prospect.* 2011;59:78–89.

[27] Minkoff SE, Stone CM, Bryant S, Peszynska M, Wheeler MF. Coupled fluid flow and geomechanical deformation modeling. *J. Pet. Sci. Eng.* 2003;38:37–56.

[28] Segura JM, Fisher QJ, Crook AJL, Dutko M, Yu J, Skachkov S, Angus DA, Verdon JP, Kendall J-M. Reservoir stress path characterization and its implications for fluid-flow production simulation. *Pet. Geosci.* 2011; 17:335–344.
[29] Prioul R, Bakulin A, Bakulin V. Nonlinear rock physics model for estimation of 3D subsurface stress in anisotropic formations: Theory and laboratory verification. *Geophysics* 2004;69:415–425.
[30] Aziz K, Settari A. *Petroleum Reservoir Simulation*. London: Applied Science Publishers Ltd.; 1979.
[31] MR Gutierrez, W Lewis, The role of geomechanics in reservoir simulation, In: Proceedings of Euro '98, 2; 1998:439–448.
[32] Rutqvist J. Determination of hydraulic normal stiffness of fractures in hard rock from hydraulic well testing. *Int. J. Rock Mech. Min. Sci. Geomech.* 1995;32:513–523.
[33] Helbig K, Rasolofosaon PNJ. A theoretical paradigm for describing hysteresis and nonlinear elasticity in arbitrary anisotropic rocks. In: *Proceedings of the Ninth International Workshop on Seismic Anisotropy: Anisotropy 2000: Fractures, Converted Waves and Case Studies*. Society of Exploration Geophysicists; 2000.
[34] Hueckel T, Cassiani G, Tao F, Pellegrino A, Fioravante V. Effect of aging on compressibility of gas/oil bearing sediments and their subsidence. *ASCE J. Geotech. Geoenviron. Eng.* 2001;127(11):926–938.
[35] Ferronato M, Castelletto N, Gambolati G, Janna C, Teatini P. II cycle compressibility from satellite measurements. *Geotechnique* 2013; 63(6):479–486.
[36] Johnson PA, Rasolofosaon PNJ. Manifestation of nonlinear elasticity in rock: Convincing evidence over large frequency and strain intervals from laboratory studies. *Nonlinear Process. Geophys.* 1996; 3:77–88.
[37] Hatchell PJ, Bourne S. Rocks under straIn: Strain-induced time-lapse time shifts are observed for depleting reservoirs. *Lead. Edge* 2005; 24:1222–1225.
[38] Crook AJL, Yu J-G, Willson SM. *Development of An Orthotropic 3D Elasticplastic Material Model for Shale*. Society of Petroleum Engineers; 2002:78238.
[39] Crook AJL, Willson SM, Yu J-G, Owen DRJ. Predictive modelling of structure evolution in sandbox experiments. *J. Struct. Geol.* 2006;28: 729–744.
[40] Angus DA, Verdon JP, Fisher QJ, Kendall J-M, Segura JM, Kristiansen TG, Crook AJL, Skachkov S, Yu J, Dutko M. Integrated fluid-flow, geomechanical and seismic modelling for reservoir characterization. *Recorder Canadian Society of Exploration Geophysicists* 2011;36(4):18–27.
[41] Nur A, Simmons G. Stress-induced velocity anisotropy in rock: An experimental study. *J. Geophys. Res.* 1969;74:6667–6674.
[42] Sayers CM. Asymmetry in the time-lapse seismic response to injection and depletion. *Geophys. Prospect.* 2007;55(5):699–705.
[43] Dewhurst DN, Siggins AF. Impact of fabric, microcracks and stress field on shale anisotropy. *Geophys. J. Int.* 2006;165:135–148.
[44] Olofsson B, Probert T, Kommedal JH, Barkved OI. Azimuthal anisotropy from the Valhall 4C 3D survey. *Lead. Edge* 2003;22: 1228–1235.
[45] Valcke S, Casey M, Lloyd G, Kendall J-M, Fisher QJ. Seismic anisotropy in sedimentary rocks. *Geophys. J. Int.* 2005;166:652–666.
[46] Kendall J-M, Fisher QJ, Covey-Crump S, Maddock J, Carter A, Hall SA, Wookey J, Valcke SLA, Casey M, Lloyd G, Ben Ismail W. Seismic anisotropy as an indicator of reservoir quality in siliciclastic rocks. *Structurally Complex Reservoirs*. In: Jolley SJ, Barr D, Walsh JJ, Knipe. R, eds. Geological Society; 2007:123–136, Special Publication 292.
[47] Schoenberg M, Sayers C. Seismic anisotropy of fractured rock. *Geophysics* 1995;60(1):204–211.
[48] Brown RJS, Korringa J. On the dependence of the elastic properties of a porous rock on the compressibility of the pore fluid. *Geophysics* 1975;40:608–616.
[49] Chapman M. Frequency-dependent anisotropy due to meso-scale fractures in the presence of equant porosity. *Geophys. Prospect.* 2003; 51:369–379.
[50] Hall SA, Kendall J-M, Maddock J, Fisher QJ. Crack density tensor inversion for analysis of changes in rock frame architecture. *Geophys. J. Int.* 2008;173:577–592.
[51] Verdon JP, Angus DA, Kendall J-M, Hall SA. The effects of microstructure and nonlinear stress on anisotropic seismic velocities. *Geophysics* 2008;73(4):D41–D51.
[52] Angus DA, Verdon JP, Fisher QJ, Kendall J-M. Exploring trends in microcrack properties of sedimentary rocks: An audit of dry-core velocity-stress measurements. *Geophysics* 2009;74:E193–E203.
[53] Kristiansen TG, Plischke B. *History Matched Full Field Geomechanics Model of the Valhall Field Including Water Weakening and Repressurasation*. SPE; 2010:131505.
[54] Ruger A. Variation of P-wave reflectivity with offset and azimuth in anisotropic media. *Geophysics* 1998;63:935–947.
[55] Hall SA, Kendall J-M. Fracture characterization at Valhall: Application of P-wave amplitude variation with offset and azimuth (AVOA) analysis to a 3D ocean-bottom data set. *Geophysics* 2003;68(4): 1150–1160.
[56] Hall SA. *Rock Fracture Characterisation and Seismic Anisotropy: Application to Ocean Bottom Seismic Data* (Ph.D. thesis), Leeds, UK: University of Leeds; 2000.
[57] Angus DA, Thomson CJ. Modelling converted seismic waveforms in isotropic and anisotropic 1-D gradients: discontinuous versus continuous gradient representations. *Stud. Geophys. Geod.* 2012;56: 383–409.
[58] Pattillo PD, Kristiansen TG, Sund GV, Kjeldstadli RM. Reservoir compaction and seafloor subsidence at Valhall. In: *Proc. Eurock '98*. Trondheim, Norway: SPE/ISRM; 1998:47274.
[59] Alam MM, Fabricius IL, Christensen HF. Static and dynamic effective stress coefficient of chalk. *Geophysics* 2012;77(2):L1–L11.
[60] B Rosland, EL Tree, P Kristiansen, Acquisition of 3D/4C OBS data at Valhall, In: 61st Annual Meeting EAGE, Expanded Abstract, E050, 1999.
[61] Barkved OI. *Seismic Surveillance for Reservoir Delivery: From a Practitioner's Point of View*. Education Tour Series, vol. 6. European Association of Geoscientists and Engineers; 2012.
[62] Zoback MD, Zinke JC. Production-induced normal faulting in the Valhall and Ekofisk oil fields. *Pure Appl. Geophys.* 2002;159:403–420.
[63] Dyer BC, Jones RH, Cowles JF, Barkved O, Folstad PG. Microseismic survey of a North Sea reservoir. *World Oil* 1999;220:74–78.
[64] Tape W, Tape C. A geometric setting for moment tensors. *Geophys. J. Int.* 2012;190(1):476–498.
[65] Teanby N, Van der Baan M, Kendall J-M. Automation of shear-wave splitting measurements using cluster analysis. *Bull. Seismol. Soc. Am.* 2004;94(2):453–463.
[66] De Meersman K, Kendall J-M, Van Der Baan M. The 1998 Valhall microseismicity: An integrated study of relocated sources, seismic multiplets and S-wave splitting. *Geophysics* 2009;74(5):183–195.
[67] AJL Crook, JG Yu, RE Flatebø, TG Kristiansen, Computational modelling of the rate dependent deformation and liquefaction of chalk, ARMA 08-176, In: The 42nd US Rock Mechanics Symposium and 2nd U.S.-Canada Rock Mechanics Symposium, held in San Francisco, 2008, June 29–July 2, 2008.
[68] Tod S. The effects of stress and fluid pressure on the anisotropy of interconnected cracks. *Geophys. J. Int.* 2002;149(1):149–156.
[69] Schubnel A, Gueguen Y. Dispersion and anisotropy of elastic waves in cracked rocks. *J. Geophys. Res.* 2003;108(B2):15.
[70] Sayers C, Kachanov M. Microcrack-induced elastic wave anisotropy of brittle rocks. *J. Geophys. Res.* 1995;100(B3):4149–4156.
[71] Jenner E. Azimuthal AVO: Methodology and data examples. *Lead. Edge* 2002;21:782–786.